The role of ionic liquid breakdown in the electrochemical metallization of VO_2: An NMR study of gating mechanisms and VO_2 reduction

Michael A. Hope,[1] Kent J. Griffith,[1] Bin Cui,[2] Fang Gao,[2] Siân E. Dutton,[3] Stuart S. P. Parkin,[2] Clare P. Grey[1,*]

[1] *Department of Chemistry, University of Cambridge, Lensfield Road, Cambridge CB2 1EW, UK.*
[2]*Max Planck Institute of Microstructure Physics, Halle (Saale) D06120, Germany.*
[3]*Cavendish Laboratory, JJ Thomson Avenue, Cambridge CB3 0HE, UK.*

Abstract

Metallization of initially insulating VO_2 *via* ionic liquid electrolytes, otherwise known as electrolyte gating, has recently been a topic of much interest for possible applications such as Mott transistors and memory devices. It is clear that the metallization takes place electrochemically and, in particular, there has previously been extensive evidence for the removal of small amounts of oxygen during ionic liquid gating. Hydrogen intercalation has also been proposed, but the source of the hydrogen has remained unclear. In this work, solid-state magic angle spinning NMR spectroscopy (^{1}H, ^{2}H, ^{17}O and ^{51}V) is used to investigate the thermal metal-insulator transition in VO_2, before progressing to catalytically hydrogenated VO_2 and electrochemically metallized VO_2. In these experiments electrochemical metallization of bulk VO_2 particles is shown to be associated with intercalation of hydrogen, the degree of which can be measured with quantitative ^{1}H NMR spectroscopy. Possible sources of the hydrogen are explored, and by using a selectively deuterated ionic liquid, it is revealed that the hydrogenation is due to deprotonation of the ionic liquid; specifically, for the commonly used dialkyl-imidazolium based ionic liquids, it is the “carbene” proton which is responsible. Increasing the temperature of the electrochemistry is shown to increase the degree of hydrogenation, forming first a less hydrogenated metallic orthorhombic phase then a more hydrogenated insulating Curie-Weiss paramagnetic orthorhombic phase, both of which were also observed for catalytically hydrogenated VO_2. The NMR results are supported by magnetic susceptibility measurements, which corroborate the degree of Pauli and Curie-Weiss paramagnetism. Finally, NMR spectroscopy is used to identify the presence of hydrogen in an electrolyte gated thin film of VO_2, suggesting that electrolyte breakdown, proton intercalation and reactions with decomposition products within the electrolyte should not be ignored when interpreting the electronic and structural changes observed in electrochemical gating experiments.

Introduction

In 1959 it was discovered that upon heating to above 67 °C, vanadium dioxide (VO_2) transitions from an insulating to a metallic state with an increase in conductivity of several orders of magnitude;[1] since then, VO_2 has been the subject of extensive study to understand the subtle interplay between electronic correlations and a Peierls distortion which underlie this metal-insulator transition (MIT).[2–4] More recently there has been interest in electronically inducing this transition (otherwise known as gating) for possible applications such as Mott transistors[5] and memory devices;[6] this research has focused on thin films of VO_2. It was reported by Nakano et al.[7] that non-thermal metallization of VO_2 films, induced by application of a gate voltage to an electrolyte at the surface of the film (Figure 1a, left), was a purely capacitive effect, whereby the ionic liquid forms a double layer at the solid–liquid interface and hence induces a large electric field in the sample. Jeong *et al*.[8] later showed that the metallization was in fact due to the electrochemical reduction of the vanadium and consequent introduction of electrons into the band structure. This reduction must be charge balanced, and Jeong *et al.* established the simultaneous creation of oxygen vacancies on the basis of ^{18}O secondary ion mass spectrometry (SIMS) data, which showed an excess of ^{18}O at the surface of devices that had been gated and reverse gated in an $^{18}O_2$ atmosphere; this is the generally accepted mechanism in the literature.[9–14] The same group later showed that oxygen plays a role in ionic liquid gating of several other oxides including WO_3, again by ^{18}O SIMS.[15] Most recently they directly observed oxygen vacancies, using in-situ transmission electron microscopy, in $SrCoO_{2.5}$ produced by electrolyte gating of $SrCoO_3$, which was accompanied by dramatic structural and magnetic changes.[16] On the other hand, Shibuya and Sawa[17] observed hydrogen intercalation by ^1H SIMS after electrolyte gating of VO_2, which could also charge balance the reduction; however, the source of hydrogen remained unclear. It is well known that ionic liquids are chemically stable over a limited voltage window and the application of voltages outside this window can lead to breakdown of the organic molecules from which the ionic liquid is composed; furthermore, the possibility of H_2O or other hydrogen-containing impurities in the ionic liquid must also be considered.

Hydrogen intercalation *via* electrolyte gating is clearly a possible mechanism of the metallization of VO_2, because metallization has also been observed after explicit hydrogenation of VO_2 by various techniques: (i) electrolytically by splitting of H_2O in a water infiltrated nanoporous glass solid electrolyte[18] or a humid-air nanogap,[19] (ii) galvanically by electrical contact with a sacrificial anode in acidic solution,[20] and (iii) catalytically *via* hydrogen spillover.[21,22] While these studies were all based on nanosized VO_2, either thin films or nanowires, hydrogenation of bulk VO_2 has also been investigated electrochemically[23] and catalytically,[24] albeit with the studies focusing on the structural rather than the electronic properties. Questions remain, including whether ionic liquid gating is associated with hydrogenation of the VO_2? If so, what is the source of hydrogen? And, most importantly, what is the cause of metallization?

Solid-state, magic angle spinning, nuclear magnetic resonance spectroscopy (MAS NMR) is a useful tool to study the metallization of VO_2 as it is an element-specific probe of both the crystal and electronic local structures.[25,26] In particular, Knight shifts are a direct measure of the local density of states at the Fermi level for the nucleus in question; they can be used to identify metallic environments and are typically temperature-dependent.[27] Paramagnetic shifts due to localized spins, on the other hand, have a strong temperature dependence.[28] These different shift mechanisms can, therefore, be used to determine the local electronic structure.

In this work, multi-nuclear NMR spectroscopy (^1H, ^2H, ^{17}O and ^{51}V) is utilized to study the crystal and electronic structure of electrochemically metallized bulk VO_2 samples and explore the mechanism of electrochemical metallization, using imidazolium-based ionic liquids that are commonly used for electrolyte gating experiments;[8–12] these NMR results are supported by X-ray diffraction (XRD),

resistivity and magnetic susceptibility measurements. First, the NMR of pristine micron-sized VO_2 particles are investigated above and below the MIT temperature, before the magnetic and electronic properties of catalytically hydrogenated VO_2 are examined. The results are compared with electrochemically reduced bulk VO_2, and the effect of increasing the temperature at which the electrochemistry is performed is investigated. To explore the source of hydrogen in these experiments, ^2H NMR measurements were performed on bulk VO_2 which was electrochemically reduced with a selectively deuterated ionic liquid; this reveals that deprotonation of the ionic liquid occurs at the voltages used in these experiments, resulting in the observed hydrogenation of VO_2. NMR spectroscopy is then used to identify intercalated hydrogen in a thin film sample of VO_2 which has been electrolyte-gated with an imidazolium-based ionic liquid, so as to allow comparison between the results obtained with bulk samples and previous thin film electrolyte gating experiments. Finally, the implications for electrolyte gating are discussed.

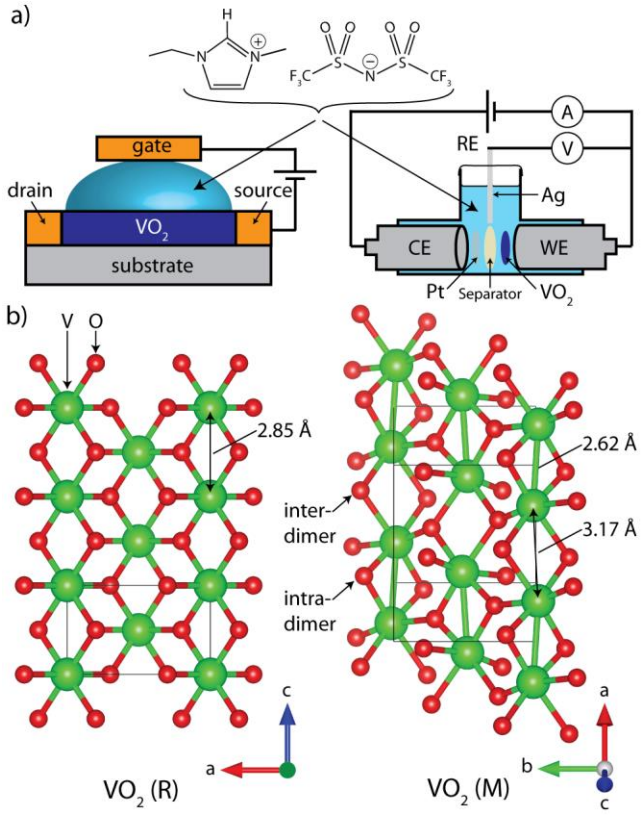

Figure 1: a) Left: schematic of a thin film electrolyte gating experiment, where a potential is applied across the gate electrode and the resistance between the source and drain is measured. Right: schematic of the three-electrode cell used in this work for electrochemical experiments on bulk VO_2 showing the VO_2 working electrode (WE), Pt counter electrode (CE) and Ag wire pseudo-reference electrode (RE); shown too is a commonly used ionic liquid, EMIm TFSI. b) Structures of the metallic, rutile, high temperature VO_2(R) phase, and the insulating, monoclinic, low temperature VO_2(M) phase. VO_2(R) has a single oxygen site in the asymmetric unit, while VO_2(M) has two oxygen sites, bridging vanadium atoms either within or between vanadium dimers.

Experimental

Synthesis: Bulk VO_2 was synthesized by comproportionating an equimolar mixture of V_2O_3 and V_2O_5 in an evacuated quartz tube at 600 °C for 48 hours to yield ~2 µm particles. The V_2O_5 (Sigma-Aldrich, 99.99%) was first dried *in vacuo* at 640 °C for four days and the V_2O_3 was synthesized by reducing V_2O_5 in 5% H_2/Ar (10 mL/min) at 650 °C for 24 hours.[29] ^{17}O-enriched VO_2 was prepared in the same way, but

starting from ^{17}O-enriched V_2O_5, which was prepared by oxidizing metallic vanadium powder (Sigma-Aldrich, 99.5%) in 70 at% $^{17}O_2$ gas (Cambridge Isotope Laboratories) at 620 °C for two days.

Catalytically hydrogenated VO_2 was prepared by mixing the comproportionated VO_2 with Pd nanoparticles (Sciventions, aqueous suspension, 1.5 mg/mL) before removing the water *in vacuo* at 100 °C to give 1 wt% Pd. The Pd/H_xVO_2 was then hydrogenated in flowing 25% H_2/N_2 at 180 °C for 15 hours. A second sample was also prepared by hydrogenation in flowing 5% H_2/Ar at 220 °C for 15 hours. Hydrogenated samples were handled in an argon glovebox.

Characterization: Powder X-ray diffraction (XRD) patterns were recorded in reflection mode with sample rotation on a PANalytical Empyrean diffractometer emitting Cu Kα (1.540598 Å + 1.544426 Å) radiation. Air-sensitive samples were packed into a Kapton sample holder. Phase identification was achieved by profile matching using PANalytical's X'Pert HighScore Plus 2.2 software and by comparison with the following ICSD entries: 1473 (V_2O_3)[30], 74705 (VO_2 M),[31] 1504 (VO_2 R)[32] and 15798 (V_2O_5).[33] Rietveld refinement was performed using the Topas Academic software package.[34] Structures were visualized with the VESTA software package.[35] Thermogravimetric analysis (TGA) was performed under flowing N_2 using a Mettler Toledo TGA/SDTA 851 thermobalance with a 100 µL Al_2O_3 crucible.

Resistivity measurements were performed on pressed pellets (750 MPa, 30 minutes, under partial vacuum) using the four-point probe technique and a Quantum Design Physical Property Measurement System (PPMS Dynacool). Susceptibility measurements were performed using a Quantum Design Magnetic Property Measurement System (MPMS3) and an applied field of 100 Oe.

Scanning electron microscopy (SEM) was performed using a TESCAN MIRA3 FEG-SEM with an acceleration voltage of 5 kV. The samples were stuck to carbon tape and coated with ~10 nm of Cr. Average particles sizes were determined from the measured images using ImageJ software.[36]

For NMR experiments, samples were packed into ZrO_2 rotors. All the NMR spectra were recorded on either a 4.70 T or a 7.05 T Bruker Avance III spectrometer, except one ^2H NMR spectrum of D_xVO_2 which was recorded on an 11.75 T Bruker Avance III spectrometer. The relatively low magnetic fields used here are advantageous for investigating the NMR of paramagnetic and metallic materials because the paramagnetic and Knight shifts are linear in the applied field, and so constant in chemical shift,[27,28] whereas the sideband separation afforded by magic angle spinning is constant in frequency; greater sideband separation, and hence resolution of signals, can therefore be achieved at lower magnetic fields for the same MAS frequency; furthermore, spinning of metallic samples is easier at lower magnetic fields. Most experiments used a Bruker 1.3 mm HX probe and either 40 kHz or 60 kHz MAS frequency, except the ^2H NMR spectra at 4.70 T and 7.05 T which used a Bruker 2.5 mm HX probe and 30 kHz MAS, the ^1H NMR spectra of the VO_2 thin film which used a Bruker 1.9 mm HX probe and 40 kHz MAS, and the wide temperature range ^1H NMR spectra of Pd/H_xVO_2 which used a Bruker 4mm HX probe and 14 kHz MAS. All experiments used a Hahn echo pulse sequence unless otherwise stated (π/2-τ-π-τ-acquire). ^1H and ^{17}O sideband separation experiments were recorded by taking the isotropic slice from a MATPASS experiment,[37] and ^1H T_1 (spin-lattice) measurements were recorded with an inversion recovery pulse sequence. ^{51}V variable offset cumulative spectra (VOCS) were recorded by summing spectra recorded with different carrier frequencies, with retuning of the probe between experiments being performed by an external automatic tuning/matching (eATM) robot.[38] Quantitative ^1H NMR spectra were recorded at 4.70 T and 60 kHz MAS, with the sample center-packed between PTFE tape to ensure excitation of the full sample mass; the integrated intensity was then compared to a calibration with known masses of adamantane, also center-packed. The T_2 relaxation constants were sufficiently long that no correction for transverse decay was required. For ^1H quantification, the catalytically hydrogenated samples were ground with a known mass of KBr to minimize skin depth penetration effects. ^1H NMR spectra of the VO_2 thin film were recorded using a DEPTH background

suppression pulse sequence (π/2-τ-π-2τ-π-τ-acquire),[39] and then background-subtracted by first recording the sample then recording the background of an empty rotor with the same experiment and taking the difference. The T_1 filtered spectrum was obtained by recording two spectra with recycle delays of 0.05 s and 0.1 s, background-subtracting both, then taking the difference, scaling the spectra so as minimize the diamagnetic signals which have longer T_1 relaxation constants.

Variable temperature NMR experiments were performed by application of heated or cooled nitrogen, with cooling achieved either with a Bruker cooling unit (BCU) or a liquid nitrogen heat exchanger. The sample temperature was determined from an *ex-situ* calibration using the temperature-dependent ^{207}Pb shift of $Pb(NO_3)_2$,[40] except for variable temperature ^{1}H spectra of catalytically hydrogenated VO_2, which was ground with KBr and the temperature measured *in-situ* from the ^{79}Br shift and T_1 constant.[41] ^{1}H NMR spectra were referenced relative to adamantane at 1.81 ppm, ^{2}H spectra to D_2O at 4.8 ppm, ^{17}O spectra to CeO_2 at 877 ppm and ^{51}V spectra to NH_4VO_3 at −571 ppm. Spectra were deconvoluted using the dmfit program.[42]

Electrochemistry: Electrochemical experiments were performed with 1-ethyl-3-methylimidazolium bis(trifluoromethylsulfonyl)imide (EMIm TFSI, Sigma Aldrich, ≥97%). The water content was determined with a Metrohm 899 Karl Fischer Coulometer to be 340 ppm as received and 34 ppm after drying *in vacuo* for two days. ½" perfluoroalkoxy (PFA) Swagelok cells were used with a Ag wire pseudo-reference electrode, platinum mesh counter electrode, glass fiber separator and stainless-steel plungers (Figure 1a, right).

Composite free-standing films were prepared comprising 80 wt% VO_2 particles, 10 wt% PTFE binder and 10 wt% conductive carbon nanoparticles to ensure good electrical contact. VO_2 was ground with carbon super P (TIMCAL) before the addition of PTFE (60 wt% dispersion in H_2O, Sigma Aldrich). Ethanol was added followed by mixing to a dough-like consistency, rolling and drying at 60 °C to yield films of 75–150 μm thickness. The electrochemical experiments were performed in air using a Bio-Logic potentiostat/galvanostat running the EC-Lab software and experiments at elevated temperatures were performed in an oven. Cells were disassembled in an argon glovebox and the VO_2 films washed with dimethyl carbonate (2 x 2.5 ml, 99.5%, anhydrous, Sigma Aldrich) before drying *in vacuo* for 20 minutes. The carbon and PTFE in the composite films make only a small and temperature independent contribution to the magnetic susceptibility.

The potential of the Ag wire pseudo-reference electrode was calibrated relative to the ferrocene-ferrocenium (Fc/Fc^+) couple by recording cyclic voltammograms of 10 mM ferrocene in EMIm TFSI at each temperature, with a scan rate of 10 mV/s (see SI §1). The potential of the reference electrode at 200 °C was extrapolated because ferrocene is not stable at this temperature.[43] The potential *vs.* Fc/Fc^+ is related to the potential *vs.* the standard hydrogen electrode (SHE) according to $E - E_{SHE} = E - E_{Fc/Fc^+} + 0.478\ \mathrm{V}$;[44] the temperature dependence of this conversion is expected to be minimal.[45]

Thin Films: Single-crystalline VO_2 films of 10×10 mm^2 area and around 200 nm thickness were deposited on (001) TiO_2 substrates by pulsed laser deposition (248 nm KrF laser) with an oxygen pressure of 0.014 mbar and a growth temperature of 400 °C. The electrolyte gating for the thin film sample was performed potentiostatically according to previously reported procedures,[8] under a vacuum of ~3×10^{-6} mbar at 280 K. The VO_2 thin film and a gold counter electrode were covered by a drop of EMIm TFSI and a gate voltage of 3 V was applied between the VO_2 thin film and the gold electrode for two hours. After gating, the ionic liquid was removed by ultrasonic cleaning in acetone and ethanol.

Results and Discussion

The Thermal Transition of Pure VO_2

The high temperature, metallic, phase of VO_2 adopts the rutile structure ($P4_2/mnm$) with the V d^1 electrons delocalized into a conduction band; the transition to the low temperature, insulating, structure is associated with a Peierls distortion to the lower symmetry monoclinic structure ($P2_1/c$), with the V d^1 electrons pairing to form V-V dimers (Figure 1b). As has been previously reported, this phase transition results in an extremely large change in shift of the ^{51}V NMR signal, from 2065 ppm in the insulating state to −3765 ppm in the metallic state (observed here for our micron-sized VO_2 particles, Figure 2a).[25,46] The positive shift is due to a Van-Vleck or orbital Knight shift, which is characteristic of an insulating state with a small bandgap, whereas the negative shift is due to an indirect or core-polarization Knight shift, which is characteristic of a metallic state where the band structure has no appreciable contribution from s orbitals at the Fermi level, as is the case in VO_2.[27] The ^{17}O NMR spectra (Figure 2b) show a similar effect: above the MIT a negative shift of −505 ppm is observed due to the core-polarization Knight shift of the metallic state, and below the MIT a positive shift is observed due to the Van-Vleck Knight shift of the insulating state. The low temperature spectrum also exhibits a splitting of the ^{17}O NMR signal due to the two crystallographically distinct oxygen sites in the lower symmetry monoclinic structure (Figure 1b): the peaks at 753 ppm and 814 ppm are tentatively assigned to the inter- and intra- vanadium dimer oxygen environments, respectively, on the basis of preliminary density functional theory (DFT) NMR shielding calculations (see SI, §2). The ^{17}O NMR spectrum of VO_2 has only previously been reported below the transition,[47] and the two signals were not assigned, but the shifts are in agreement with those found here. Note that the observed ^{17}O NMR shifts are not corrected for the second order quadrupolar shift, which from the DFT calculations is expected to contribute around −10 ppm to the observed shift at this field, based on the quadrupolar coupling constants of ~1.6 MHz.

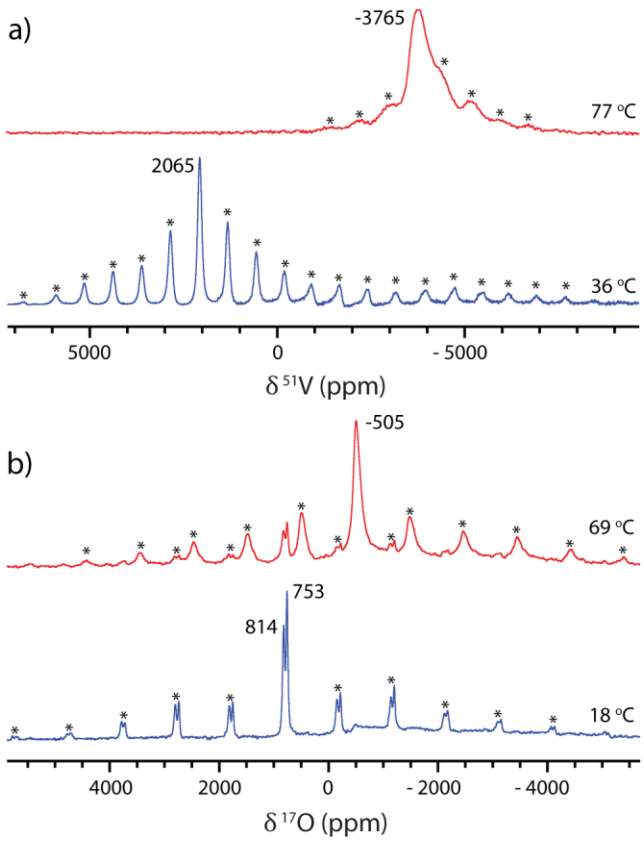

Figure 2: a) ^{51}V and b) ^{17}O NMR spectra of VO_2 above and below the MIT, recorded at 7.05 T with a Hahn echo pulse sequence. Spinning sidebands have been marked with an asterisk and the spectra have been scaled to give comparable intensities, rather than being quantitatively comparable. The ^{51}V NMR spectra were recorded at 60 kHz MAS, summing two spectra

recorded with carrier frequencies of 2000 ppm and −4750 ppm. The ^{17}O NMR spectra were recorded at 40 kHz MAS. Some of the insulating phase remains in the high temperature ^{17}O NMR spectra, and vice versa*, due to spinning induced temperature gradients within the rotor and the finite width of the MIT.*

Catalytic Hydrogenation

In order to explore the crystal and electronic structures of hydrogenated VO_2 and the resultant NMR signatures, catalytically hydrogenated VO_2 was prepared following the method of Filinchuk et al.[24] *via* catalytic spillover from palladium nanoparticles. Following hydrogenation at 180 °C, a hydrogen content determined from thermogravimetric analysis (TGA) of x = 0.365 was obtained (see SI §3). Rietveld refinement using the powder X-ray diffraction (XRD) pattern showed the presence of a small amount of unreacted VO_2 and a mixture of two orthorhombic phases (Pnnm), one with a larger unit cell and orthorhombic distortion than the other (with ratios for the *a* and *b* cell parameters of b/a = 1.112 and 1.036, respectively, see SI §4). Other than the orthorhombic distortion, the orthorhombic phases have the same structure as the high temperature VO_2 rutile phase (Figure 1b, left).

This result is in contrast to that of Filinchuk et al. who only found the orthorhombic phase with the smaller unit cell, which they denoted O1, after hydrogenation at 190 °C. However, Chippindale et al.[23] showed that both the size of the unit cell and the orthorhombic distortion scaled with the degree of hydrogenation x, suggesting that the second phase identified in our work is a more hydrogenated analogue of the first. Modifying the notation of Filinchuk et al., the less and more hydrogenated orthorhombic phases will be referred to as O1a and O1b respectively. Using the relationship between the orthorhombic distortion and the hydrogen content reported by Chippindale et al.,[23] the hydrogen content of both phases can be predicted, which combined with the phase fractions determined from Rietveld analysis (see SI §4) results in a total hydrogen content of $x = 0.42(7)$ for this sample (Table 1). This is in reasonable agreement with that determined by TGA.

Four-point resistivity measurements of pressed pellets of VO_2 and Pd/H_xVO_2 (Figure 3a) clearly show the MIT in pristine VO_2 at 340 K. This is almost completely suppressed in Pd/H_xVO_2 (the MIT of the residual unreacted VO_2 can, however, still just be seen); furthermore, the resistivity of the Pd/H_xVO_2 is ~500 times lower than insulating VO_2, although the temperature dependence still has semiconducting character rather than being fully metallic (this may be due to residual Mott localization at this degree of reduction). Zero-field cooled susceptibility measurements (Figure 3b) corroborate the resistivity data: the Pd/H_xVO_2 exhibits an increased temperature-dependent susceptibility due to the Pauli paramagnetism of the metallic phase, as well as suppression of the MIT, although there is also an increased Curie paramagnetic component, which is indicative of localized spins.

The ^{51}V NMR spectrum (Figure 3c) confirms the presence of vanadium atoms in a metallic environment in Pd/H_xVO_2, with almost complete loss of the insulating VO_2 peak at 2065 ppm and the appearance of a resonance at negative shift, as seen for pure VO_2 above the MIT; however, the signal in this case is very broad and the spinning sidebands cannot be resolved, which is most likely due to a greater distribution of local vanadium environments in the less uniform H_xVO_2 sample. The ^1H MAS NMR spectrum of Pd/H_xVO_2 contained a series of overlapping signals and thus a MATPASS sideband separation pulse sequence was used so that only the isotropic resonances are seen[37] (Figure 3d); the spectrum shows two signals centered around 110 ppm and 445 ppm, as well as a diamagnetic peak around 0 ppm, which is ascribed to ubiquitous diamagnetic hydrogen-containing impurities.

To aid assignment of the ^1H spectrum, a second sample of Pd/H_xVO_2 was synthesized at 220 °C and found from XRD to have a greater phase fraction of O1b (36 wt% *c.f.* 12 wt% for the sample synthesized at 180 °C). The ^1H NMR spectrum of this sample had a correspondingly greater intensity for the 445

ppm signal, allowing the 115 and 445 ppm regions to be assigned to O1a and O1b respectively (see SI §5).

Variable temperature ^{1}H NMR spectra show that the shift of the O1b phase has a Curie-Weiss temperature dependence (see SI §6), indicating that this phase is paramagnetic, the shift originating from localized electrons, with the unpaired electron density in the V t_{2g} orbital partially delocalizing into the H 1s orbital *via* a 90° π delocalization mechanism.[48] These localized electron spins suggest that this phase is insulating, as also recently found for highly catalytically hydrogenated thin films of HVO_2 (x = 1);[21] the insulating state in this case is shown to arise from the large degree of hydrogenation which causes the lattice to expand, reducing the overlap between the vanadium d orbitals and hence reducing the valence bandwidth so that there is Mott localization of the electrons, as for the insulating phase of pristine VO_2. The O1a resonance, on the other hand, does not show a Curie-Weiss temperature dependence so the major interaction responsible for this signal is likely a Knight shift, indicating that this phase is metallic; this is a positive, direct contact Knight shift because the only valence orbital for hydrogen is the 1s orbital. These assignments are corroborated by measurements of the ^{1}H T_1 relaxation constants: ~0.03 s for O1a and ~0.002 s for O1b (see SI §7); both phases relax much more quickly than diamagnetic protons (typically ~1–10 s), and the localized paramagnetic O1b signal relaxes an order of magnitude faster than the metallic O1a signal, as expected.

These NMR experiments thus confirm the Curie and Pauli components identified in the magnetic susceptibility measurements. The amount of hydrogenation could also be determined with quantitative ^{1}H NMR spectroscopy, which yielded hydrogen contents for the two phases which are in reasonable agreement with the TGA and XRD results (Table 1), further corroborating the assignments.

To summarize, catalytic hydrogenation of VO_2 yielded two orthorhombic phases: a less hydrogenated, metallic, Pauli paramagnetic phase denoted O1a; and a more hydrogenated, Curie-Weiss paramagnetic phase denoted O1b; the hydrogen content of both were determined by analysis of the unit cell parameters and by quantitative ^{1}H NMR spectroscopy.

Table 1: Comparison of the sample hydrogen content (x in H_xVO_2), and its distribution between the two orthorhombic phases, as determined by thermogravimetric analysis (TGA), Rietveld refinement of the XRD pattern and quantitative ^{1}H NMR spectroscopy. The average hydrogen content of the sample is determined from the XRD data by taking the product of the O1a/O1b phase fraction (%) and the phase hydrogen content predicted from the orthorhombic distortion. The error in the last digit is shown in brackets. Discrepancies between the XRD and NMR quantifications are discussed in the SI, see §4.

	TGA	XRD	NMR
O1a		86 % × 0.33(5) = 0.28(5)	0.19(2)
O1b		12 % × 1.1(1) = 0.14(3)	0.17(2)
Total	0.365(3)	0.42(7)	0.36(3)

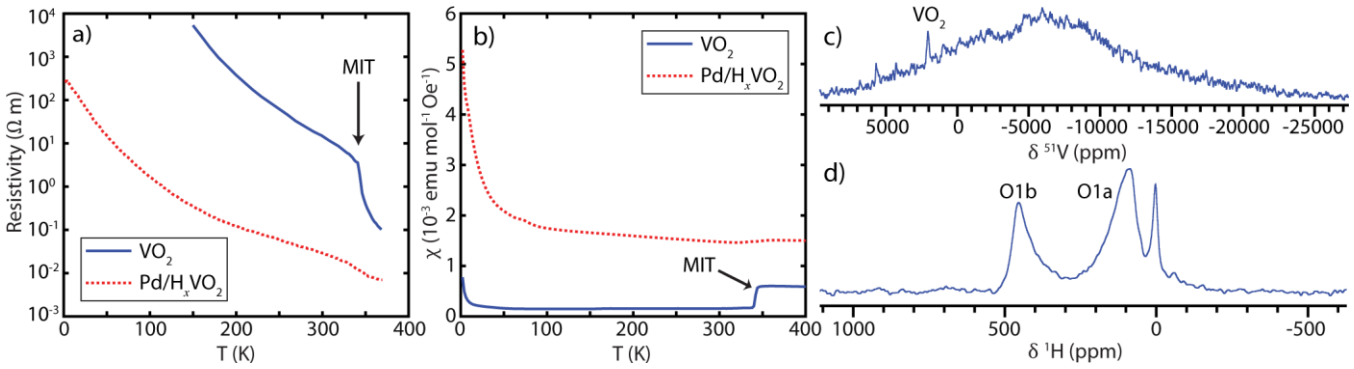

Figure 3: a) Resistivity and b) zero field cooled magnetic susceptibility of VO_2 before and after catalytic hydrogenation, and c) ^{51}V and d) ^{1}H NMR spectra of the catalytically hydrogenated VO_2. The ^{51}V NMR spectrum was recorded at 4.70 T, 60 kHz MAS and a sample temperature of ~50 °C, using a Hahn echo pulse sequence and variable offset cumulative spectra (VOCS) acquisition. Spectra were acquired in steps of 5000 ppm between carrier frequencies of 5000 ppm and −20000 ppm and summed to produce the spectrum shown above. The residual signal due to insulating VO_2 at 2065 ppm is indicated. The ^{1}H NMR spectrum is the isotropic slice of a 2D MATPASS sideband separation spectrum, which was recorded at 4.70 T, 40 kHz MAS and a sample temperature of ~30 °C.

Electrochemical Hydrogenation – Room Temperature

Having studied the thermal MIT in pure VO_2 and the effect of catalytic hydrogenation, electrochemical metallization of VO_2 was investigated. The experiments were performed on bulk VO_2, using ~15 mg free-standing composite films, made with standard battery/supercapacitor electrode preparation techniques. Unlike previous potentiostatic electrolyte gating experiments,[7–14,17] here galvanostatic reduction was used, so that the energetics of different processes could be inferred from the potential, which was measured relative to a silver wire pseudo-reference electrode (Figure 1a, right). The use of the reference electrode avoids electrode polarization effects and allows the potential of the insertion reaction to be measured relative to a known potential, which is particularly important in this case because the reaction that occurs at the counter electrode has not been established definitively. The ionic liquid used was 1-ethyl-3-methylimidazolium bis(trifluoromethylsulfonyl)imide (EMIm TFSI, Figure 1a, top)—a standard electrolyte used in electrolyte gating experiments—and the counter electrode was platinum mesh. A specific current of 6.46 mA g^{-1} was applied for 50 h, which, assuming 100% Coulombic efficiency, corresponds to one electron transferred per vanadium atom (Figure 4a).

After performing the electrochemistry, the cell was disassembled under inert atmosphere and the VO_2 electrode was characterized *ex-situ*. The presence of protons in a metallic environment is clearly revealed via the observation of a resonance at 110 ppm in the ^{1}H NMR spectrum (Figure 4c); a second peak is observed at approximately 0 ppm, which is ascribed to protons in diamagnetic local environments, from imperfect washing of the electrolyte, electrolyte breakdown products and other hydrogen-containing impurities. Quantification of the ^{1}H NMR spectrum, however, yields a hydrogen content of only x = 0.037, despite charge corresponding to one electron per vanadium ion being transferred. Examination of the electrochemistry shows that the electrochemical potential (Figure 4a) initially decreases before reaching a plateau at around −1.6 V *vs.* Fc/Fc^{+}. A second sample was prepared where the electrochemistry was stopped after transferring 0.075 electrons per vanadium, *i.e.* at the beginning of the plateau; this sample had an essentially identical hydrogen content of x = 0.035, which shows that the plateau does not correspond to the hydrogenation reaction, but rather a competing side reaction that prevents further hydrogenation. Electrochemical reduction of VO_2 in an organic electrolyte was previously found to compete with hydrogen evolution,[23] *i.e.* the hydrogen evolves as H_2 rather than intercalating into the VO_2 (the origin of the hydrogen will be discussed later); this is likely to be the case here, given that the voltage falls below the hydrogen evolution voltage in EMIm TFSI (−0.07 V vs. Fc/Fc^{+}), although hydrogen evolution can be negligible until much lower

voltages depending on the catalytic properties of the electrode and the source of the hydrogen.[49] Alternative side reactions could also include cation or anion decomposition.[50]

The XRD pattern of the electrochemically reduced VO_2 shows that the structure remains monoclinic, but with a lattice expansion consistent with a small degree of hydrogenation (see SI §4). The ^{51}V NMR spectrum confirms that the monoclinic, insulating, VO_2 phase dominates (Figure 4d); the sharp resonance of this phase, at 2065 ppm, and the associated spinning sidebands likely obscure any broad signal due to vanadium in a metallic environment. The susceptibility of this sample (Figure 4b) shows an increase in both the Curie and Pauli paramagnetic susceptibilities relative to VO_2, although not as much as for the catalytically hydrogenated sample, and the MIT can still be observed, albeit broadened and suppressed to a lower temperature (332 K on heating *c.f.* 342 K in pristine VO_2). The susceptibility also exhibits spin glass-like behavior below $T_f \approx 150$ K: there is a significant difference between the zero-field cooled (ZFC) and field cooled (FC) susceptibility traces and the ZFC susceptibility increases with temperature below T_f (after the Curie contribution has sufficiently decreased);[51] spin glass-like behavior was further confirmed by hysteresis in the magnetization *vs.* field measurements (see SI §8).

^{17}O NMR spectra were recorded on a sample of ^{17}O-enriched VO_2, reduced electrochemically in the same way (Figure 4e). In the spectrum recorded below the MIT temperature, the insulating monoclinic VO_2 resonances at 753 and 814 ppm are seen as expected. Then in the spectrum recorded above the MIT, the negatively Knight shifted signal of the metallic phase is again observed, but at the more negative shift of −550 ppm, compared to −505 ppm for pristine metallic VO_2 (see SI §9 for a direct comparison of these spectra). This is evidence of the electron (n-type) doping associated with hydrogen intercalation, which increases the density of states at the Fermi level by both raising the Fermi level and increasing the overlap of the V d orbitals; the greater density of states at the Fermi level then increases the magnitude of the Knight shift.

These results suggest localized metallization, as may be expected for low electron doping levels,[4] but not complete metallization; unfortunately, resistivity measurements of these films are not possible due to the conductive carbon and the low density, so the degree of metallization must be inferred. Metallic nanodomains have previously been observed in pure VO_2 just below the MIT,[52] and could also explain the behavior observed here for H_xVO_2 with a low level of hydrogenation: there is a Knight shift for the ^1H nuclei, indicating that the hydrogen is in a metallic environment, but the whole sample cannot have been metallized because the ^{51}V NMR spectrum is dominated by vanadium in an insulating environment. Furthermore, metallic nanodomains can also result in cluster glass behavior, with ferromagnetic coupling within domains but weak and disordered coupling between domains, which would explain the spin glass-like effects observed in the magnetic measurements.

To determine whether the galvanostatic experiments performed here would yield the same results as previous two-electrode potentiostatic electrolyte gating experiments, a bulk VO_2 sample was electrochemically reduced potentiostatically by applying a voltage of −2.5 V between the Pt counter electrode and the VO_2 working electrode (see SI §10). Hydrogen in a metallic environment is again observed by ^1H NMR, although quantitative NMR yields a lower hydrogen content of $x = 0.016$; this is ascribed to the smaller applied voltage than in the galvanostatic experiment, where it reaches −3.6 V. Nevertheless, potentiostatic electrochemical reduction of bulk VO_2 clearly also results in hydrogenation.

Since the previous electrolyte gating experiments were observed to be reversible,[7,8] a bulk VO_2 sample was electrochemically reduced galvanostatically for 24 hours before reversing the current for 24 hours (see SI §11); the ^1H NMR then shows no H_xVO_2 signal, indicating that the electrochemical hydrogenation is also reversible.

The localized/incomplete metallization achieved for bulk VO_2 at room temperature is in contrast to the previously reported complete metallization observed for thin film samples. One possible explanation for this difference is the strain present in epitaxial thin films grown on TiO_2 (001) substrates; the strain favors the metallic state, as evidenced by the reduction of the thermal MIT temperature to −3 °C.[11] However, for VO_2 grown on Al_2O_3 $(10\bar{1}0)$ substrates there is minimal strain and the MIT is observed at 67 °C as for bulk VO_2, yet full metallization is still achieved in electrolyte gating experiments;[8] this suggests that strain is not necessary for metallization. Instead, this could be a kinetic effect: due to the small sample volume in a thin film and the shorter diffusion distances, a greater degree of electrochemical reduction could be achieved before competing side reactions limit the reaction. This is supported by the observation of Passarello et al.[12] that complete suppression of the MIT could not be achieved for 1 µm bars of VO_2, whereas it could be achieved for 0.5 µm bars in the same setup; the average VO_2 particle size here as determined by SEM is 1.9 µm (see SI §12), which could explain the lack of complete metallization observed. This is corroborated by the results of electrochemical reduction of ~30 nm VO_2 nanoparticles (see SI §13), which show a greater hydrogenation of x = 0.20 from ^{1}H NMR.

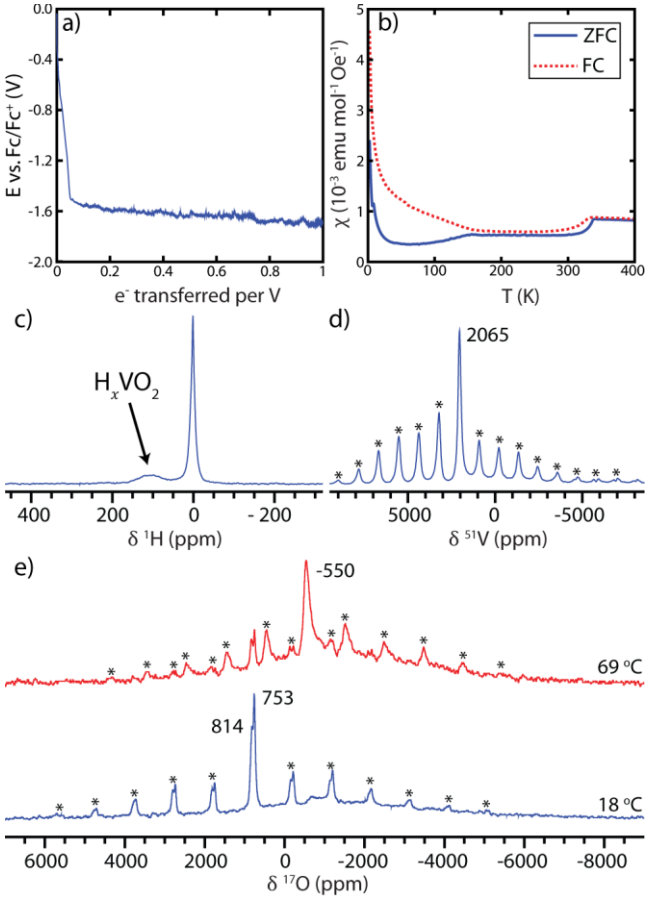

Figure 4: a) voltage profile; b) zero-field cooled (ZFC) and field cooled (FC) magnetic susceptibilities; and c) ^{1}H, d) ^{51}V and e) ^{17}O NMR spectra of VO_2 after electrochemical reduction at room temperature. The ^{1}H NMR spectrum is the isotropic slice of a 2D MATPASS sideband separation spectrum which was recorded at 4.70 T, 40 kHz MAS and a sample temperature of ~30 °C. The ^{51}V VOCS NMR spectrum was recorded at 4.70 T, 60 kHz MAS and a sample temperature of ~50 °C using a Hahn echo pulse sequence and variable offset cumulative spectra (VOCS) acquisition with carrier frequencies from 5000 ppm to −20000 ppm in steps of 5000 ppm (although only the region of interest is shown here). The ^{17}O NMR spectra were recorded at 7.05 T, 40 kHz MAS and a sample temperature of ~30 °C. Spinning sidebands are indicated with an asterisk.

Electrochemical Hydrogenation – Elevated Temperature

The electrochemistry was subsequently performed at elevated temperatures in an attempt to achieve a greater extent of electrochemical hydrogenation. For temperatures up to 150 °C, the degree of

hydrogenation increased (Figure 5a), forming the same orthorhombic phases observed for catalytic hydrogenation, first O1a then O1b, as shown by ^{1}H NMR spectroscopy (Figure 5c) and Rietveld refinement of the XRD patterns (Figure 5b). The ^{51}V NMR spectra (Figure 5d) further show progressive loss of the insulating VO_2 resonance at 2065 ppm and appearance of broad features at negative shifts, which correspond to vanadium ions in a metallic environment. $V^{(0)}$ and V^{5+} impurities can also be seen in the ^{51}V NMR spectra for the samples electrochemically hydrogenated at 100 °C and 150 °C, which are negligible by XRD but are much more readily observed via ^{51}V NMR spectroscopy since the signals are noticeably sharper than those of the H_xVO_2 phases. The susceptibility data corroborate these results; Figure 5e shows the Curie and Pauli paramagnetic components as fitted from the low temperature tail and the high temperature asymptote respectively (see SI §14). As expected, the Pauli paramagnetism increases for samples prepared at up to 150 °C due to the increasing hydrogenation, which is accompanied by the addition of electrons, increasing the density of states at the Fermi level; the Curie paramagnetism also increases for the samples prepared at 100 °C and 150 °C due to the localized paramagnetic O1b phase. The ^{17}O NMR spectra recorded for ^{17}O enriched samples also reflect the progressive formation of O1a and then O1b with increasing temperature up to 150 °C, with the paramagnetic O1b phase being identifiable from the Curie-Weiss temperature dependence of the ^{17}O shift (see SI §15).

The greater electrochemical hydrogenation at higher temperatures could be due to a number of factors. One consideration is that above 67 °C the pristine VO_2 is in the metallic rutile phase, which will afford better electrical contact between particles in the electrode as well as presumably reducing the barrier to formation of the orthorhombic phases which are structurally more similar; indeed, no monoclinic phase remains after performing the electrochemistry at 100 °C and above. However, the amount of hydrogenation appears to increase systematically with temperature, rather than there being a step change between the 50 °C and 100 °C samples.

A second explanation is that the differences in the activation energies of the hydrogenation reaction and the limiting side reaction(s) will result in different temperature dependences of the reaction rates; the potential of the plateau in the electrochemistry becomes less negative with increasing temperature (see SI §16), which indicates that the limiting process becomes more facile and hence a change in the kinetics. In particular, the rate of hydrogen diffusion will increase at higher temperatures, reducing the overpotential required to drive the hydrogenation reaction. By 200 °C the degree of hydrogenation is reduced again, which is presumably because the competing side reactions have now become faster again relative to the hydrogenation reaction; see SI §17 for a more detailed discussion of this sample.

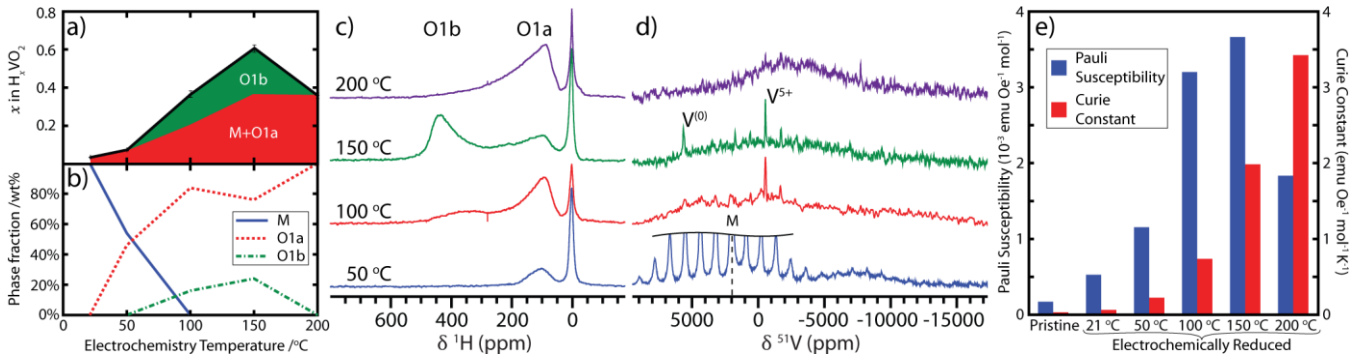

Figure 5: Characterization of VO_2 electrochemically hydrogenated between 50 °C and 200 °C: a) the hydrogen content determined from quantitative ^{1}H NMR spectroscopy; b) the phase fractions of the monoclinic (M) and two orthorhombic phases (O1a and O1b) determined from Rietveld analysis of the powder XRD; the c) ^{1}H and d) ^{51}V NMR spectra; and e) the Pauli and Curie paramagnetic components of the magnetic susceptibility. The ^{1}H NMR spectra in (c) represent the isotropic

slices of the MATPASS spectra which were recorded at 4.70 T, 40 kHz MAS and a sample temperature of ~30 °C; note that these spectra are not quantitative. The ^{51}V NMR spectra in (d) were recorded at 4.70 T, 60 kHz MAS and a sample temperature of ~50 °C using a Hahn echo pulse sequence and variable offset cumulative spectra (VOCS) acquisition with carrier frequencies from 5000 ppm to −20000 ppm in steps of 5000 ppm. The Pauli component of the susceptibility is taken as the susceptibility measured at 300 K, to avoid any contribution from the MIT, and the Curie constant, C, was found by fitting the low temperature tail to the function $\chi = \frac{C}{T-\Theta} + \chi_0$, where Θ is the Weiss constant and χ_0 is the temperature-independent paramagnetism.

Electrolyte Gating of Thin Films

To compare the electrochemical metallization experiments on bulk VO_2 with the previous studies on thin films, a 200 nm VO_2 film was grown on a 0.5 mm TiO_2 (001) substrate and electrolyte gated with EMIm TFSI; the film was then crushed and lightly hand ground with a mortar and pestle to allow it to be packed into an NMR sample rotor. As the film cannot be separated from the substrate, there is a 2500-fold dilution of the sample which makes recording the ^{1}H NMR spectrum challenging, and the ^{51}V NMR spectrum essentially impossible using the current substrates. The conventional background-subtracted ^{1}H NMR spectrum (Figure 6, top) is dominated by diamagnetic impurities, either from the TiO_2 substrate or the sample surface, obscuring any signal from the gated VO_2. However, by applying a T_1 filter, the diamagnetic resonances can be largely removed as they relax more slowly (Figure 6, bottom); this leaves signals that relax more quickly, such as metallic H_xVO_2 environments with T_1 ~ 0.03 s. Indeed, in the T_1 filtered ^{1}H NMR spectrum a resonance can be observed at 115 ppm, where metallic H_xVO_2 was observed in the electrochemically metallized bulk samples. The same signal was not observed in the T_1 filtered ^{1}H NMR spectrum of a VO_2 thin film before electrolyte gating (see SI §18). Although these experiments are approaching the sensitivity limits of NMR spectroscopy, this suggests that electrolyte gating experiments of thin films also result in hydrogenation of the VO_2, due to ionic liquid breakdown.

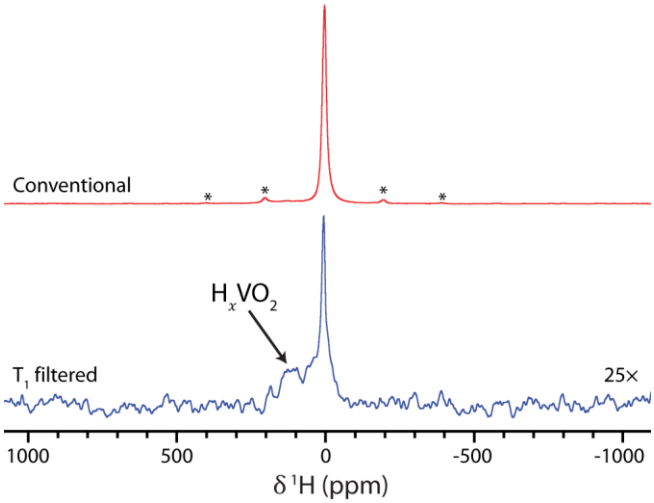

Figure 6: ^{1}H NMR spectra of a 200 nm VO_2 thin film on 0.5 mm TiO_2 after electrolyte gating, recorded at 4.70 T, 40 kHz MAS and a sample temperature of ~40 °C, with spinning sidebands marked by asterisks. The conventional spectrum was obtained with a recycle delay of 0.05 s using a DEPTH pulse sequence[39] and subtracting the background. The T_1 filtered spectrum was recorded by taking the difference between background-subtracted spectra with recycle delays of 0.05 s and 0.1 s, scaling the spectra so as to remove as much as possible the diamagnetic signals. The spectra with recycle delays of 0.05 s were recorded with 2.72 million scans each for the sample and the background, and the spectra with recycle delays of 0.1 s were recorded with 0.68 million scans.

Electrochemical Hydrogenation – Mechanism

Having established that VO_2 can be hydrogenated electrochemically with an ionic liquid electrolyte, the obvious question is: where does the hydrogen come from? One possibility could be electrolysis of H_2O which is invariably present in ionic liquids due to their hygroscopic nature,[53] given that

hydrogenation of VO_2 by water electrolysis has previously been demonstrated.[18,19] However, even after drying the ionic liquid under vacuum for 2 days, electrochemical reduction of VO_2 at 100 °C still gave a similar level of hydrogenation, with a greater hydrogen content than can be explained by the water content (1.9 µmol of water in the ionic liquid as determined by Karl Fischer titration, 27 µmol of hydrogen in the electrochemically hydrogenated VO_2). Another potential source of hydrogen is the ionic liquid itself, and for 1,3-dialkyl-imidazolium ionic liquids, such as EMIm TFSI, the most acidic proton is the "carbene" proton between the nitrogen atoms of the imidazolium cation, so-called because on deprotonation it forms an N-heterocyclic carbene which is stabilized by the adjacent nitrogen lone pairs[54] (Figure 7a); this deprotonation is driven by the low potential at the VO_2 during reduction.[50]

To test this hypothesis, a sample of EMIm TFSI was prepared where the carbene proton had been selectively exchanged for deuterium; this was achieved by stirring EMIm TFSI in excess D_2O at 50 °C for 24 hours before drying off the D_2O *in vacuo.* A ~90 at% isotopic substitution in the ionic liquid was confirmed by ^1H and ^2H NMR spectroscopy (see SI §19). Performing the electrochemical hydrogenation at 100 °C with the selectively deuterated ionic liquid decreased the ^1H content of the H_xVO_2 accordingly, as determined by ^1H NMR spectroscopy. The ^2H NMR spectrum (Figure 7b) then shows deuterium incorporated in both the O1a and O1b environments, as well as a sharp signal at 0 ppm, due again to diamagnetic decomposition products; the quadrupolar ^2H nucleus gives rise to a large sideband manifold which can be modelled to find the nuclear quadrupolar coupling constant, see SI §20. This provides compelling evidence that it is the carbene hydrogen of the EMIm TFSI ionic liquid that is intercalated into the VO_2 upon electrochemical reduction. The breakdown of the ionic liquid is also evident when removing the ionic liquid after an experiment: for electrochemical reduction at room temperature, the originally clear ionic liquid becomes strongly discolored, and at higher temperatures it becomes dark brown.

Further evidence for this mechanism is seen by using ionic liquids with different imidazolium-based cations, for which the observed potential correlates with the acidity of the protons (see SI §21). For electrolyte gating with non-imidazolium-based ionic liquids, it seems likely that hydrogen intercalation is also involved in the electrochemical metallization of VO_2; indeed, for diethylmethyl(2-methoxyethyl)ammonium bis(trifluoromethylsulfonyl)imide (DEME TFSI), another commonly used ionic liquid for electrolyte gating experiments,[7,14,17] hydrogenation is also observed after electrochemical reduction (see SI §22). However, the mechanism of hydrogen abstraction must be different for non-imidazolium-based ionic liquids: this will be the subject of future investigation. To determine the onset voltage of VO_2 hydrogenation, bulk VO_2 composite films were electrochemically reduced as a function of potential (see SI §23); hydrogenation was first observed at −0.53 V vs. Fc/Fc^+, which is much less negative than the reported cathodic stability limit of EMIm TFSI on a glassy carbon electrode, −2.5 V,[55] but this is not surprising given that VO_2 both partakes in and catalyses the ionic liquid decomposition.

This work should be contrasted with that of Lu et al. who performed similar electrochemical hydrogenation experiments, now using thin films of $SrCoO_{2.5}$ and the ionic liquids EMIm BF_4 and DEME TFSI.[56] They added D_2O to the ionic liquids before heating to 100 °C and then performed the electrochemistry; they subsequently observed ^2H ions from SIMS in the gated material and therefore concluded that the hydrogen arose from H_2O (D_2O) in the ionic liquid. Although this is a different material, it is possible that the heating caused exchange of the labile proton on the ionic liquid for deuterium, and hence that the hydrogenation is also due to decomposition of the ionic liquid in this case. However, further investigation would be required to unambiguously determine the source of hydrogen in this different system, in particular because the potential at which the oxide is reduced may be important in determining the mechanism of hydrogenation.

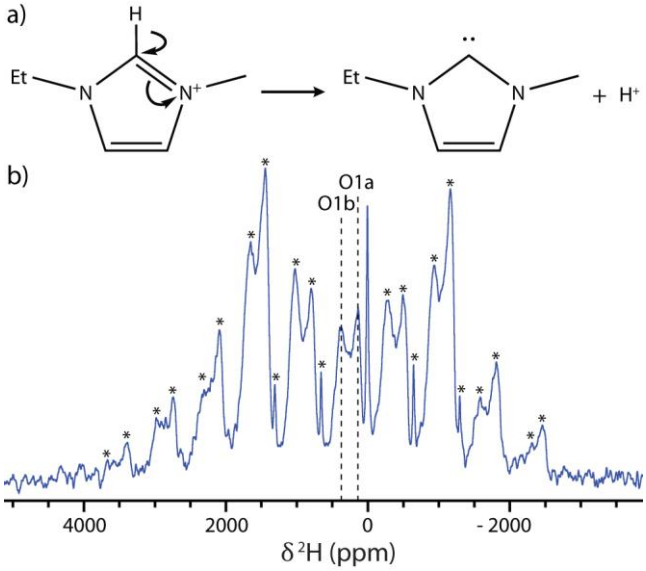

Figure 7: a) Deprotonation of the "carbene hydrogen" in the EMIm cation. b) The ^2H NMR spectrum of VO_2 after electrochemical metallization with EMIm TFSI which has had the carbene hydrogen exchanged for deuterium, showing signals from both O1a and O1b D_xVO_2. The spectrum was recorded at 7.05 T, 30 kHz MAS and a sample temperature of ~40 °C using a Hahn echo pulse sequence. Spinning sidebands are shown with asterisks.

The experiments on the electrochemical reduction of VO_2 presented here do not rule out the presence of oxygen vacancies, but they suggest that hydrogenation could be a sufficient explanation for the metallization, particularly for certain classes of ionic liquids and if large overpotentials (gating voltages) are used. The electrochemical reaction of the VO_2 in this case is

$$\mathrm{VO_2} + x\mathrm{H^+} + xe^- \rightarrow \mathrm{H}_x\mathrm{VO_2} \qquad [1]$$

However, even in systems where oxygen vacancies dominate, such as WO_3 and $SrCoO_{2.5}$,[15,16,56] we propose that hydrogen still plays an important role in the electrochemistry; this hydrogen would most likely come from decomposition of the ionic liquid, although as discussed above, the balance between water and electrolyte decomposition may depend on both the system and the applied potential. The charge balancing of metal reduction in the metal oxide MO_n by loss of oxygen could be written as

$$\mathrm{MO}_n \rightarrow \mathrm{MO}_{n-x} + \frac{x}{2}\,\mathrm{O_2} \qquad [2]$$

However, this above formulation of the process is too simplistic because it is a purely chemical reaction and O_2 cannot be generated at the anode (where the reduction occurs). Instead the proposed reaction must occur by two electrochemical half-reactions, at the negative (metal oxide) and positive (gate/counter) electrodes respectively:

$$\mathrm{MO}_n + 2xe^- \rightarrow \mathrm{MO}_{n-x} + x\mathrm{O^{2-}} \qquad \text{(Negative electrode) [3]}$$

$$x\mathrm{O^{2-}} \rightarrow \frac{x}{2}\mathrm{O_2} + 2xe^- \qquad \text{(Positive electrode) [4]}$$

Transport of O^{2-} between the electrodes is formally required, which we suggest could occur as H_2O, formed from the protons liberated *via* electrolyte decomposition, rather than as a free O^{2-} ion. *I.e.*

$$\mathrm{MO}_n + 2x\mathrm{H^+} + 2xe^- \rightarrow \mathrm{MO}_{n-x} + x\mathrm{H_2O} \qquad \text{(Negative electrode) [5]}$$

$$x\mathrm{H_2O} \rightarrow \frac{x}{2}\mathrm{O_2} + 2x\mathrm{H^+} + 2xe^- \qquad \text{(Positive electrode) [6]}$$

This reaction has direct analogies with the onset of so-called conversion reactions in battery electrodes where Li_2O is generated along with the reduction of the metal ions, eventually to the metal (e.g. $CoO + 2Li^+ + 2e^- \rightarrow Co + Li_2O$).[57,58] Note that these conversion reactions can also commence with lithiation (intercalation) before conversion, which is again analogous to the proton intercalation observed here in VO_2.

Conclusions

Electrochemical metallization of micron-sized VO_2 particles with imidazolium ionic liquids has been shown to be associated with intercalation of protons and concomitant reduction of the V^{4+} ions, ^1H NMR spectra with a positive Knight shift due to the metallization providing a clear signature of this event. There is also evidence for the same hydrogenation in thin films of VO_2, after light grinding into small pieces so as to pack into the sample container. In the case of 1,3-dialkyl-imidazolium-based ionic liquids, which are common for previously reported electrolyte gating experiments, the hydrogenation is due to deprotonation of the ionic liquid, specifically the "carbene" hydrogen of the imidazolium cation; this has been shown by selectively substituting this hydrogen for deuterium.

Electrochemical reduction of bulk VO_2 at room temperature does not afford complete metallization, but rather localized metallization in the vicinity of the intercalated H, which is in contrast to thin film electrolyte gating experiments; greater hydrogenation could, however, be achieved for nanoparticulate VO_2. Increasing the temperature of the electrochemistry also yields greater hydrogenation, forming first a metallic orthorhombic phase and then a second localized paramagnetic orthorhombic phase with a greater degree of hydrogenation; a schematic phase diagram for H_xVO_2 is shown in Figure 8. A mixture of the same orthorhombic phases was also observed for catalytically hydrogenated VO_2, for which the resistivity was shown to decrease by a factor of 500 compared to pristine VO_2. The degree of hydrogenation can be measured by quantitative ^1H NMR spectroscopy, and the Pauli and Curie paramagnetic components of the two orthorhombic phases can be tracked *via* ^1H, ^{17}O and ^{51}V NMR spectroscopy; in particular, the ^{17}O Knight shift in the metallic phase is a sensitive probe of the density of states at the Fermi level and hence the degree of electron doping, and variable temperature experiments for both ^1H and ^{17}O can be used to assign the Curie paramagnetic phases.

These results should be taken into consideration when developing a device based on electrolyte gating of VO_2 thin films: the carbene species formed on deprotonation of the ionic liquid is very reactive and will cause decomposition of the electrolyte; this is not a sustainable long-term reaction. However, if hydrogenation is the cause of the metallization, an alternative electrochemical system can be formulated to intentionally and reversibly intercalate hydrogen, which could allow the practical realization of electrolyte gating in devices. Finally, our results suggest that the protons produced by electrolyte degradation may be involved in oxygen extraction mechanisms in this and other electrochemically-gated systems, a proposal that is currently under investigation.

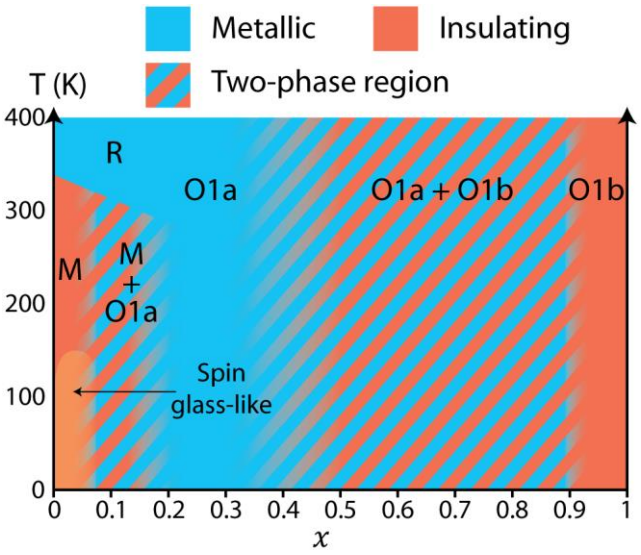

Figure 8: Schematic phase diagram of H_xVO_2, showing the monoclinic (M), rutile (R) and two orthorhombic phases (O1a and O1b), with two phase regions cross hatched. Boundaries were estimated from the compositions of the H_xVO_2 samples studied in this work, rather than being rigorously mapped. The M and O1b phases are insulating while the R and O1a phases are metallic. The single-phase rutile (R) region for $x \approx 0.1$ above the MIT temperature was determined by variable temperature XRD, see SI §24.

Acknowledgements

M.A.H. would like to thank the Oppenheimer Foundation for funding. K.J.G. gratefully acknowledges support from The Winston Churchill Foundation of the United States, the Herchel Smith Scholarship and the EPSRC (EP/MO09521/1). S.S.P.P., B.C. and F.G. acknowledge partial funding from the EU H2020 program "Phase Change Switch". B.C. thanks the Alexander von Humboldt Foundation for their support. Finally, we would like to thank all the members of the Grey Group who provided help, advice and discussion for this work.

Supporting information.
Additional experiments as referenced in the text are supplied as Supporting Information.

References

(1) Morin, F. J. Oxides Which Show a Metal-to-Insulator Transition at the Neel Temperature. *Phys. Rev. Lett.* **1959**, *3* (1), 34–36.

(2) Goodenough, J. B. The Two Components of the Crystallographic Transition in VO2. *J. Solid State Chem.* **1971**, *3* (4), 490–500.

(3) Rice, T. M.; Launois, H.; Pouget, J. P. Comment on "VO2: Peierls or Mott-Hubbard? A View from Band Theory." *Phys. Rev. Lett.* **1994**, *73* (22), 3042–3042.

(4) Khomskii, D. I. *Transition Metal Compounds*; Cambridge University Press: Cambridge, 2014.

(5) Chudnovskiy, F.; Luryi, S.; Spivak, B. Switching Device Based on First-Order Metal- Insulator Transition Induced by External Electric Field. *Futur. Trends Microelectron. Nano Millenn.* **2002**, 148–155.

(6) Driscoll, T.; Kim, H. T.; Chae, B. G.; Di Ventra, M.; Basov, D. N. Phase-Transition Driven Memristive System. *Appl. Phys. Lett.* **2009**, *95* (4), 93–96.

(7) Nakano, M.; Shibuya, K.; Okuyama, D.; Hatano, T.; Ono, S.; Kawasaki, M.; Iwasa, Y.; Tokura, Y. Collective Bulk Carrier Delocalization Driven by Electrostatic Surface Charge Accumulation. *Nature* **2012**, *487* (7408), 459–462.

(8) Jeong, J.; Aetukuri, N.; Graf, T.; Schladt, T. D.; Samant, M. G.; Parkin, S. S. P. Suppression of Metal-Insulator Transition in VO2 by Electric Field-Induced Oxygen Vacancy Formation. *Science* **2013**, *339* (6126), 1402–1405.

(9) Chen, S.; Wang, X. J.; Fan, L.; Liao, G.; Chen, Y.; Chu, W.; Song, L.; Jiang, J.; Zou, C. The Dynamic Phase Transition Modulation of Ion-Liquid Gating VO2 Thin Film: Formation, Diffusion, and Recovery of Oxygen Vacancies. *Adv. Funct. Mater.* **2016**, *26* (20), 3532–3541.

(10) Gupta, S. N.; Pal, A.; Muthu, D. V. S.; Anil Kumar, P. S.; Sood, A. K. Metallic Monoclinic Phase in VO2 Induced by Electrochemical Gating: In Situ Raman Study. *EPL* **2016**, *115* (1), 17001.

(11) Jeong, J.; Aetukuri, N. B.; Passarello, D.; Conradson, S. D.; Samant, M. G.; Parkin, S. S. P. Giant Reversible, Facet-Dependent, Structural Changes in a Correlated-Electron Insulator Induced by Ionic Liquid Gating. *Proc. Natl. Acad. Sci.* **2015**, *112* (4), 1013–1018.

(12) Passarello, D.; Altendorf, S. G.; Jeong, J.; Rettner, C.; Arellano, N.; Topuria, T.; Samant, M. G.; Parkin, S. S. P. Evidence for Ionic Liquid Gate-Induced Metallization of Vanadium Dioxide Bars over Micron Length Scales. *Nano Lett.* **2017**, *17* (5), 2796–2801.

(13) Dahlman, C. J.; LeBlanc, G.; Bergerud, A.; Staller, C.; Adair, J.; Milliron, D. J. Electrochemically Induced Transformations of Vanadium Dioxide Nanocrystals. *Nano Lett.* **2016**, *16* (10), 6021–6027.

(14) Singh, S.; Abtew, T. A.; Horrocks, G.; Kilcoyne, C.; Marley, P. M.; Stabile, A. A.; Banerjee, S.; Zhang, P.; Sambandamurthy, G. Selective Electrochemical Reactivity of Rutile VO2 towards the Suppression of Metal-Insulator Transition. *Phys. Rev. B* **2016**, *93* (12), 1–8.

(15) Altendorf, S. G.; Jeong, J.; Passarello, D.; Aetukuri, N. B.; Samant, M. G.; Parkin, S. S. P. Facet-Independent Electric-Field-Induced Volume Metallization of Tungsten Trioxide Films. *Adv. Mater.* **2016**, *28* (26), 5284–5292.

(16) Cui, B.; Werner, P.; Ma, T.; Zhong, X.; Wang, Z.; Taylor, J. M.; Zhuang, Y.; Parkin, S. S. P. Direct Imaging of Structural Changes Induced by Ionic Liquid Gating Leading to Engineered Three-Dimensional Meso-Structures. *Nat. Commun.* **2018**, *9* (1), 3055.

(17) Shibuya, K.; Sawa, A. Modulation of Metal-Insulator Transition in VO2 by Electrolyte Gating-Induced Protonation. *Adv. Electron. Mater.* **2016**, *2* (2), 1500131.

(18) Katase, T.; Endo, K.; Tohei, T.; Ikuhara, Y.; Ohta, H. Room-Temperature-Protonation-Driven On-Demand Metal-Insulator Conversion of a Transition Metal Oxide. *Adv. Electron. Mater.* **2015**, *1* (7), 1500063.

(19) Sasaki, T.; Ueda, H.; Kanki, T.; Tanaka, H. Electrochemical Gating-Induced Reversible and Drastic Resistance Switching in VO2 Nanowires. *Sci. Rep.* **2015**, *5* (1), 17080.

(20) Chen, Y.; Wang, Z.; Chen, S.; Ren, H.; Wang, L.; Zhang, G.; Lu, Y.; Jiang, J.; Zou, C.; Luo, Y. Non-Catalytic Hydrogenation of VO2 in Acid Solution. *Nat. Commun.* **2018**, *9* (1), 818.

(21) Yoon, H.; Choi, M.; Lim, T.-W.; Kwon, H.; Ihm, K.; Kim, J. K.; Choi, S.-Y.; Son, J. Reversible Phase Modulation and Hydrogen Storage in Multivalent VO2 Epitaxial Thin Films. *Nat. Mater.* **2016**, *15* (10), 1113–1119.

(22) Wei, J.; Ji, H.; Guo, W.; Nevidomskyy, A. H.; Natelson, D. Hydrogen Stabilization of Metallic Vanadium Dioxide in Single-Crystal Nanobeams. *Nat. Nanotechnol.* **2012**, *7* (6), 357–362.

(23) Chippindale, A. M.; Dickens, P. G.; Powell, A. V. Synthesis, Characterization, and Inelastic Neutron Scattering Study of Hydrogen Insertion Compounds of VO2(Rutile). *J. Solid State Chem.* **1991**, *93* (2), 526–533.

(24) Filinchuk, Y.; Tumanov, N. A.; Ban, V.; Ji, H.; Wei, J.; Swift, M. W.; Nevidomskyy, A. H.; Natelson, D. In Situ Diffraction Study of Catalytic Hydrogenation of VO2 : Stable Phases and Origins of Metallicity. *J. Am. Chem. Soc.* **2014**, *136* (22), 8100–8109.

(25) Gro Nielsen, U.; Skibsted, J.; Jakobsen, H. J. β-VO2—a V(IV) or a Mixed-Valence V(III)–V(V) Oxide—studied by 51V MAS NMR Spectroscopy. *Chem. Phys. Lett.* **2002**, *356* (1–2), 73–78.

(26) Lynch, G. .; Segel, S. .; Sayer, M. Nuclear Magnetic Resonance Study of Polycrystalline VO2. *J. Magn. Reson.* **1974**, *15* (1), 8–18.

(27) Bennett, L. H.; Watson, R. E.; Carter, G. C. Relevance of Knight Shift Measurements to the Electronic Density of States. *J. Res. Natl. Bur. Stand. Sect. A Phys. Chem.* **1970**, *74A* (4), 569.

(28) Pell, A. J.; Pintacuda, G.; Grey, C. P. Paramagnetic NMR in Solution and the Solid State. *Prog. Nucl. Magn. Reson. Spectrosc. (in press)*.

(29) *Gmelins Handbuch Der Anorganischen Chemie, Vanadium, Vol: B1*, 8th ed.; Chemie gmbh weinheim/bergstr, 1967.

(30) Rice, C. E.; Robinson, W. R. Structural Changes in the Solid Solution (Ti1−xVx)2O3 as x Varies from Zero to One. *J. Solid State Chem.* **1977**, *21* (2), 145–154.

(31) Rogers, K. D. An X-Ray Diffraction Study of Semiconductor and Metallic Vanadium Dioxide. *Powder Diffr.* **1993**, *8* (4), 240–244.

(32) Ghedira, M.; Vincent, H.; Marezio, M.; Launay, J. C. Structural Aspects of the Metal-Insulator Transitions in V0.985Al0.015O2. *J. Solid State Chem.* **1977**, *22* (4), 423–438.

(33) Bachmann, H.G.; Ahmed, F.R.; Barnes, W. H. The Crystal Structure of Vanadium Pentoxide. *Zeitschrift fuer Krist. Krist. Krist. Krist.* **1961**, *115*, 110–131.

(34) Coelho, A. A. Indexing of Powder Diffraction Patterns by Iterative Use of Singular Value Decomposition. *J. Appl. Crystallogr.* **2003**, *36* (1), 86–95.

(35) Momma, K.; Izumi, F. VESTA 3 for Three-Dimensional Visualization of Crystal, Volumetric and Morphology Data. *J. Appl. Crystallogr.* **2011**, *44* (6), 1272–1276.

(36) Schneider, C. A.; Rasband, W. S.; Eliceiri, K. W. NIH Image to ImageJ: 25 Years of Image Analysis. *Nat. Methods* **2012**, *9* (7), 671.

(37) Hung, I.; Zhou, L.; Pourpoint, F.; Grey, C. P.; Gan, Z. Isotropic High Field NMR Spectra of Li-Ion Battery Materials with Anisotropy >1 MHz. *J. Am. Chem. Soc.* **2012**, *134* (4), 1898–1901.

(38) Pecher, O.; Halat, D. M.; Lee, J.; Liu, Z.; Griffith, K. J.; Braun, M.; Grey, C. P. Enhanced Efficiency of Solid-State NMR Investigations of Energy Materials Using an External Automatic Tuning/Matching (EATM) Robot. *J. Magn. Reson.* **2017**, *275*, 127–136.

(39) Robin Bendall, M.; Gordon, R. E. Depth and Refocusing Pulses Designed for Multipulse NMR with Surface Coils. *J. Magn. Reson.* **1983**, *53* (3), 365–385.

(40) Bielecki, A.; Burum, D. P. Temperature Dependence of 207 Pb MAS Spectra of Solid Lead Nitrate. An Accurate, Sensitive Thermometer for Variable-Temperature MAS. *J. Magn. Reson. Ser. A* **1995**, *116*, 215–220.

(41) Thurber, K. R.; Tycko, R. Measurement of Sample Temperatures under Magic-Angle Spinning from the Chemical Shift and Spin-Lattice Relaxation Rate of 79Br in KBr Powder. *J. Magn. Reson.* **2009**, *196* (1), 84–87.

(42) Massiot, D.; Fayon, F.; Capron, M.; King, I.; Le Calvé, S.; Alonso, B.; Durand, J.-O.; Bujoli, B.; Gan, Z.; Hoatson, G. Modelling One- and Two-Dimensional Solid-State NMR Spectra. *Magn.*

Reson. Chem. **2002**, *40* (1), 70–76.

(43) De Souza, A. C.; Pires, A. T. N.; Soldi, V. Thermal Stability of Ferrocene Derivatives and Ferrocene-Containing Polyamides. *J. Therm. Anal. Calorim.* **2002**, *70* (2), 405–414.

(44) Bizzarri, C.; Conte, V.; Floris, B.; Galloni, P. Solvent Effects of Ionic Liquids: Investigation of Ferrocenes as Electrochemical Probes. *J. Phys. Org. Chem.* **2011**, *24* (4), 327–334.

(45) Matsumiya, M.; Terazono, M.; Tokuraku, K. Temperature Dependence of Kinetics and Diffusion Coefficients for Ferrocene/Ferricenium in Ammonium-Imide Ionic Liquids. *Electrochim. Acta* **2006**, *51* (7), 1178–1183.

(46) Umeda, J. J.; Kusumoto, H.; Narita, K.; Yamada, E. Nuclear Magnetic Resonance in Polycrystalline VO2. *J. Chem. Phys.* **1965**, *42* (1965), 1458.

(47) Bastow, T. J.; Stuart, S. N. 17O NMR in Simple Oxides. *Chem. Phys.* **1990**, *143* (3), 459–467.

(48) Carlier, D.; Ménétrier, M.; Grey, C. P.; Delmas, C.; Ceder, G. Understanding the NMR Shifts in Paramagnetic Transition Metal Oxides Using Density Functional Theory Calculations. *Phys. Rev. B* **2003**, *67* (17), 174103.

(49) Meng, Y.; Aldous, L.; Belding, S. R.; Compton, R. G. The Hydrogen Evolution Reaction in a Room Temperature Ionic Liquid: Mechanism and Electrocatalyst Trends. *Phys. Chem. Chem. Phys.* **2012**, *14* (15), 5222.

(50) DeVos, N.; Maton, C.; Stevens, C. V. Electrochemical Stability of Ionic Liquids: General Influences and Degradation Mechanisms. *ChemElectroChem* **2014**, *1* (8), 1258–1270.

(51) Mydosh, J. A. *Spin Glasses: An Experimental Introduction*; Taylor & Francis: London, 1993.

(52) Qazilbash, M. M.; Brehm, M.; Chae, B.-G.; Ho, P.-C.; Andreev, G. O.; Kim, B.-J.; Yun, S. J.; Balatsky, A. V; Maple, M. B.; Keilmann, F.; Kim, H.-T.; Basov, D. N. Mott Transition in VO2 Revealed by Infrared Spectroscopy and Nano-Imaging. *Science* **2007**, *318* (5857), 1750–1753.

(53) Krannich, M.; Heym, F.; Jess, A. Characterization of Six Hygroscopic Ionic Liquids with Regard to Their Suitability for Gas Dehydration: Density, Viscosity, Thermal and Oxidative Stability, Vapor Pressure, Diffusion Coefficient, and Activity Coefficient of Water. *J. Chem. Eng. Data* **2016**, *61* (3), 1162–1176.

(54) Hollóczki, O.; Gerhard, D.; Massone, K.; Szarvas, L.; Németh, B.; Veszprémi, T.; Nyulászi, L. Carbenes in Ionic Liquids. *New J. Chem.* **2010**, *34* (12), 3004.

(55) Mousavi, M. P. S.; Dittmer, A. J.; Wilson, B. E.; Hu, J.; Stein, A.; Bühlmann, P. Unbiased Quantification of the Electrochemical Stability Limits of Electrolytes and Ionic Liquids. *J. Electrochem. Soc.* **2015**, *162* (12), A2250–A2258.

(56) Lu, N.; Zhang, P.; Zhang, Q.; Qiao, R.; He, Q.; Li, H.-B.; Wang, Y.; Guo, J.; Zhang, D.; Duan, Z.; Li, Z.; Wang, M.; Yang, S.; Yan, M.; Arenholz, E.; Zhou, S.; Yang, W.; Gu, L.; Nan, C.-W.; Wu, J.; Tokura, Y.; Yu, P. Electric-Field Control of Tri-State Phase Transformation with a Selective Dual-Ion Switch. *Nature* **2017**, *546* (7656), 124–128.

(57) Poizot, P.; Laruelle, S.; Grugeon, S.; Dupont, L.; Tarascon, J.-M. Nano-Sized Transition-Metal Oxides as Negative-Electrode Materials for Lithium-Ion Batteries. *Nature* **2000**, *407* (6803), 496–499.

(58) Yamakawa, N.; Jiang, M.; Grey, C. P. Investigation of the Conversion Reaction Mechanisms for Binary Copper(II) Compounds by Solid-State NMR Spectroscopy and X-Ray Diffraction. *Chem. Mater.* **2009**, *21* (14), 3162–3176.

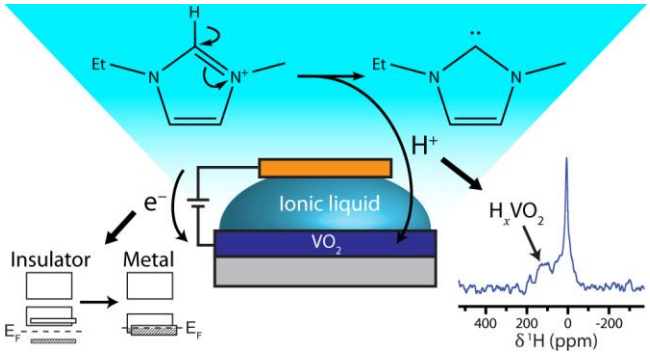
H
Et
N
N+
Et
N
N
H+
e−
Ionic liquid
VO2
HxVO2
Insulator
Metal
EF
EF
400
200
0
-200
δ 1H (ppm)